Design optimization and lab demonstration of ZELDA, a Zernike sensor for near-coronagraph quasi-static measurements

Mamadou N'Diaye[a]*, Kjetil Dohlen[b], Amandine Caillat[b], Anne Costille[b], Thierry Fusco[b,c], Aïssa Jolivet[b,d], Fabrice Madec[b], Laurent Mugnier [c], Baptiste Paul[b,c], Jean-François Sauvage[b,c], Rémi Soummer[a], Arthur Vigan[b], J. Kent Wallace[e]

[a] Space Telescope Science Institute, 3700 San Martin Drive, Baltimore, MD 21218, USA
[b] Aix Marseille Université, CNRS, LAM UMR 7326, 13388 Marseille, France
[c] ONERA, 29 avenue de la Division Leclerc, 92322 Châtillon, France
[d] Institut d'Astrophysique et de Géophysique, Allée du 6 août, 4000 Liège 1, Belgium
[e] Jet Propulsion Laboratory, 4800 Oak Grove Drive, Pasadena, CA 91109, USA

ABSTRACT

The exoplanet direct imagers Gemini/GPI and VLT/SPHERE are built around extreme adaptive optics (ExAO) to correct the atmospheric turbulence and the aberrations associated with the optical surfaces. However, additional strategies are necessary to correct the non-common path aberrations (NCPA) between the ExAO and science paths that can limit the instrument contrast performance. To perform an adequate calibration, we have developed ZELDA, a Zernike sensor to achieve NCPA measurements with nanometric accuracy. We report the results of a new design analysis that maximizes the dynamic range, and from laboratory demonstrations on the LAM high-contrast testbed and on VLT/SPHERE during its integration.

Keywords: high angular resolution, coronagraphy, wavefront sensing, wavefront control

1. INTRODUCTION

The instruments Palomar/P1640,[1] Gemini/GPI,[2] and VLT/SPHERE[3] have recently been deployed on ground-based telescopes to directly image and extract the spectrum of warm or massive, gaseous exoplanets which are 10^5 to 10^7 times fainter than their host bright star in the near-infrared. These instruments use extreme adaptive optics (ExAO) to compensate for the atmospheric turbulence and coronagraphy to suppress the star diffraction due to the telescope aperture.

However, the contrast performance of these instruments is limited by the presence of non-common path aberrations (NCPA) existing between the ExAO and the science path of the instruments. These residual aberrations produce a halo of speckles in the coronagraphic field, making the observation of companions 10^6 times fainter than their host bright star very challenging. NCPA are typically of the order of a few tens of nanometers and require a calibration with nanometric accuracy to observe companions of one order of magnitude fainter.[4] With SPHERE, a pointing error smaller than 0.5 mas rms was specified to ensure a satisfying centering of the star image on the coronagraph and reach the scientific objectives of the instrument.[5] Results of recent on-sky tests have showed excellent agreement with these requirements.[6]

Several post processing methods have been proposed to remove these speckles over the past few years.[7–12] Instrumental concepts have also been developed to measure NCPA, relying on classical or coronagraphic phase diversity methods,[13–15] interferometric approaches,[16–18] speckle nulling and wavefront control techniques[19–21] or analysis of the light blocked by a coronagraph.[22,23] The Zernike sensor and its different flavors[24–27] also constitutes a promising option to measure these small errors with the adequate accuracy. We have developed the Zernike Sensor for Extremely Low-level Differential Aberrations (ZELDA) to perform NCPA measurements

*E-mail: mamadou@stsci.edu

with nanometric accuracy in high-contrast imaging instruments,[28] see Figure 1. Based upon the Zernike phase-contrast techniques, this sensor uses a focal plane phase mask to produce interference between a reference wave created by the mask and the phase errors present in the system. As a result, this sensor converts the aberrations in the entrance pupil into intensity variations in the exit pupil.

To prepare for future potential upgrade of the current exoplanet direct imagers, we analyze the properties of ZELDA to develop new designs with a maximized dynamic range, see Section 2. In our previous communications, we reported first experimental results on the LAM high-contrast testbed,[29] and we pursue our efforts with the development of a closed-loop system, see Section 3. Work on ZELDA in VLT/SPHERE[30] has also been persued, and very interesting first results obtained during installation of the instrument at Paranal with a new mask providing larger dynamic range are reported in Section 4. We finally discuss the next steps of the project.

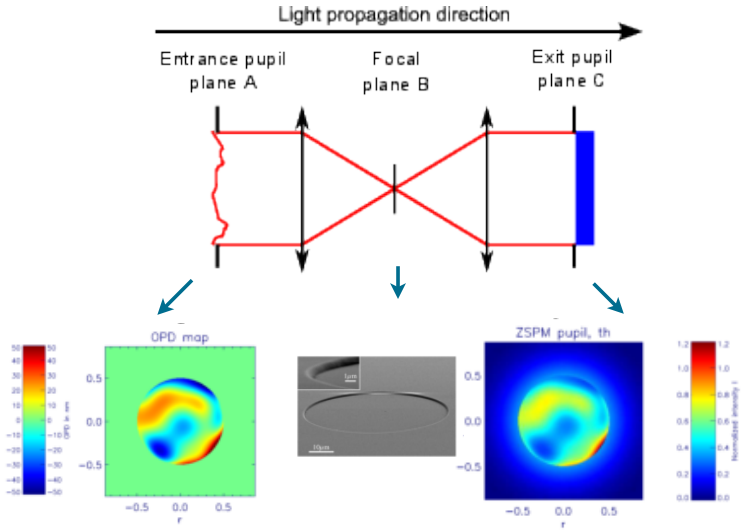

Figure 1. Basic illustration of the ZELDA concept. Phase aberrations in the entrance pupil (left) are coded as intensity variations in the exit pupil (right) thanks the interference with the reference wave created by diffraction at the Zernike phase mask (centre).

2. ZELDA PROPERTIES

ZELDA performs a phase-to-intensity conversion that depends on the mask characteristics, i.e. the diameter d and the depth which is related to the sensor phase delay θ. The principle and formalism of this Zernike sensor were detailed in N'Diaye et al.[28] We here derive some interesting properties from the formalism presented in this paper to design new masks according to the specific application. In the following, λ and D denote the wavelength and the diameter of the telescope aperture. We recall the expression of the ZELDA signal I_C as a function of the phase error φ for a given pixel in the entrance pupil:

$$I_C = P^2 + 2b^2(1-\cos\theta) + 2Pb\left[\sin\varphi\sin\theta - \cos\varphi(1-\cos\theta)\right] . \quad (1)$$

where P and b denote the amplitude pupil function and the amplitude diffracted by the focal plane phase mask of diameter d. The term θ represents the phase shift introduced by the mask.

For a typical mask size $d = 1.06\,\lambda/D$, a phase shift $\theta = \pi/2$ and considering a normalized amplitude in the entrance pupil $P = 1$, b ranges between 0.4 and 0.6 (see N'Diaye et al. Figure 3). In the following, we assume $\theta = \pi/2$, $P = 1$ and $b = 0.5$. The previous expression simplifies as follows:

$$I_C = 1 + 0.5(1-\cos\theta) + \left[\sin\varphi\sin\theta - \cos\varphi(1-\cos\theta)\right] . \quad (2)$$

Figure 2 shows the ZELDA signal as a function of the wavefront error for a given pixel, considering masks with three different optical path difference (OPD). The intensity received by a pixel depends on the WFE on the

location of that pixel with a sinusoidal function. However, the sinusoid is not symmetric about zero aberration, giving rise to an asymmetric dynamic range defined by the monotonic range around zero. The limits of the dynamic range is given by the changes of gradient sign of I_C, i.e. $dI_C/d\varphi = 0$. In the case of a classical $\pi/2$ mask depth (OPD=$\lambda/4$), the dynamic of the sensor ranges between $-\lambda/8$ and $3\,\lambda/8$, as illustrated with the added arrows in Figure 2.

This intensity function also varies with the mask design: a shallow mask has a symetrized dynamic range but with reduced sensitivity (falling to zero for zero depth), and a deep mask, tending towards a Roddier & Roddier phase mask coronagraph,[31–33] has reduced range, but a flux level at zero WFE tending towards zero so that the photon noise associated with the detection of very low aberration levels could be made small. These interesting aspects must be taken into account in the design of such sensors according to the specific application.

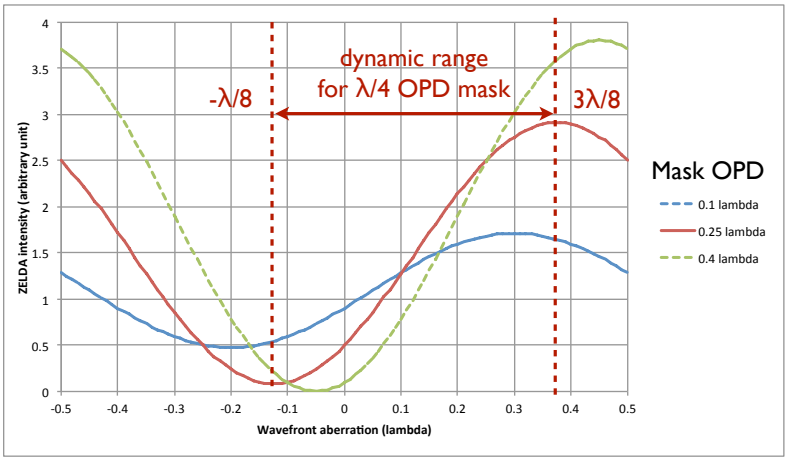

Figure 2. ZELDA pupil intensity as a function of phase aberration for a given pixel. Intensity is normalized with respect to the pupil intensity in the absence of mask. Curves are showed for different values of phase mask delay (values in the legend indicate mask OPD in λ). The dynamic range for the $\lambda/4$ phase delay mask is underlined in this plot, showing that phase ranging between $-\lambda/8$ and $3\,\lambda/8$ can theoretically be measured with this mask design.

3. LABORATORY DEMONSTRATION

ZELDA has been implemented on the High Dynamic-range Imaging testbed at LAM (Figure 3) and a first experiment demonstrating its capacity to correct wavefront deformations in closed loop was conducted.[30] In this setup, ZELDA received a beam coming from an adaptive optics system based on an ALPAO deformable mirror (DM), with a 5.5 mm pupil covering the central 5x5 actuators of the 9x9 actuators mirror.

ZELDA measured the wavefront at a rate of about 0.1 Hz and calculated the corresponding slope map which was fed back to the AO loop in the form of wavefront sensor reference slopes thanks to a specially made Matlab interface. Calculation of the slope map was done using a control matrix obtained by singular value decomposition (SVD) of the influence functions, made by imposing positive and negative pokes on the DM actuators. Convergence towards a flat wavefront with less than 9 nm rms residual wavefront error was reached within two iterations, see Figure 4. Figure 5 shows the original and final wavefront as estimated by ZELDA. This experiment allowed us to demonstrated the functionality of the sensor and its capacity to work in closed loop together with an AO system.

4. PRELIMINARY RESULTS OF A PROTOTYPE IN VLT/SPHERE

As part of a strategy to improve SPHERE performance by implementing high-order NCPA calibration as a future upgrade path, a prototype ZELDA mask has been installed in the infrared coronagraph wheel. A first version was tested during initial assembly in France, but tests indicated that this mask, using a deep design with a small dynamic range (see Section 2) was not suitable for practical operation in SPHERE.[30]

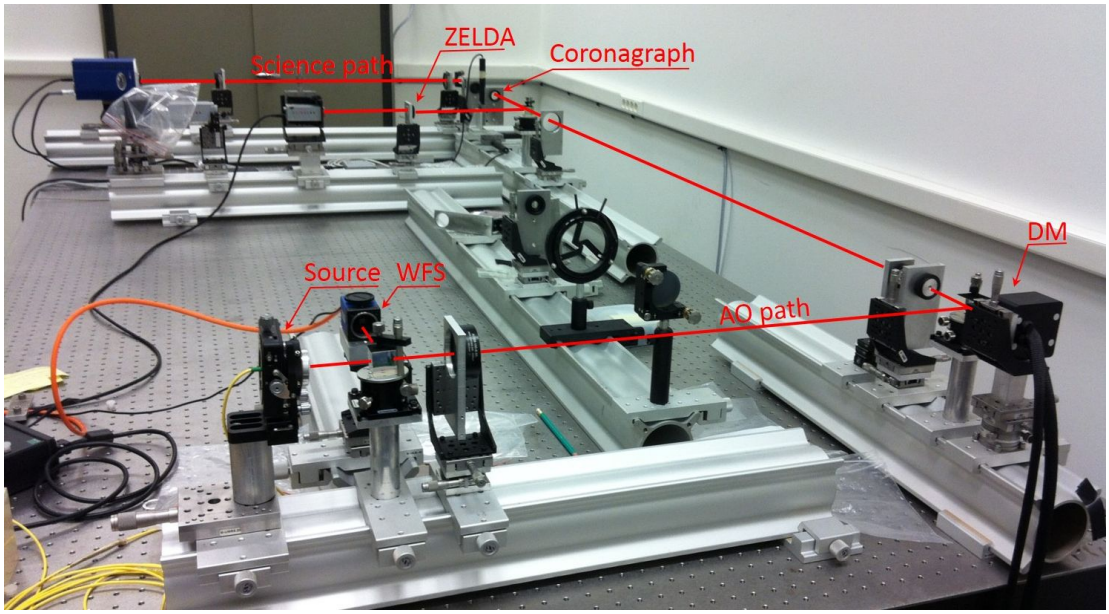

Figure 3. The LAM High Dynamic range Imaging testbed. In the foreground, the source, deformable mirror, and wavefront sensor operate in closed loop, launching an AO-corrected beam towards the coronagraph. Just before arriving at the coronagraph, a beamsplitter sends part of the flux towards the Zernike mask and the ZELDA camera. In the science path, the coronagraph is followed by a Lyot stop and a high-dynamic camera.

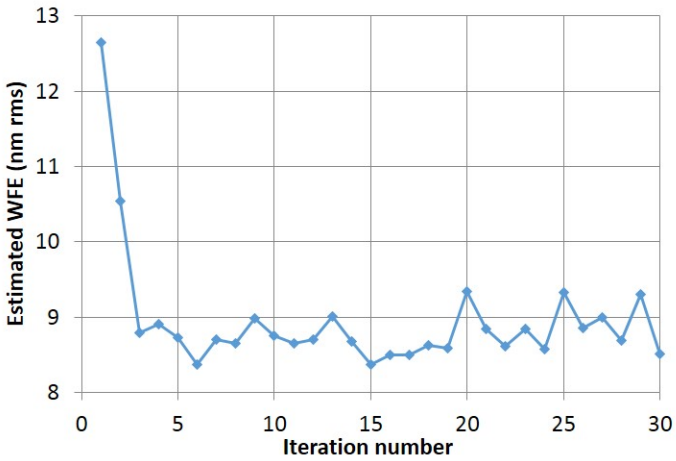

Figure 4. Convergence of the wavefront error while running ZELDA as an on-line calibration sensor for a 5x5 actuator adaptive optics loop. With initial calibration errors set to 13 nm, the final performance of below 9 nm was reached in two iterations.

A new prototype was therefore manufactured and installed during integration of the instrument at Paranal in April 2014. We here report on preliminary tests made before the first commissioning run of SPHERE in May 2014. The new mask was designed to provide a larger dynamic range (200nm negative range in the H band instead of 60nm) than the one original prototype thanks to a shallower mask profile ($0.22\lambda/D$ instead of $0.42\lambda/D$), and was hence expected to be more linear and tolerant to NCPA, and less affected by dead actuators in the DM.

By varying the reference slopes of the differential tip-tilt sensor located just in front of the coronagraph wheel, the image of an internal point source was scanned across the ZELDA mask. A tilt ramp was thus created with steps of 0.5 to 1 pixel of 12.5 mas (0.3λ/D at 1600nm). Analysis of these data was first done pixel-by pixel, creating wavefront maps scaled in nm using the mathematical framework developed earlier.[28] These maps were

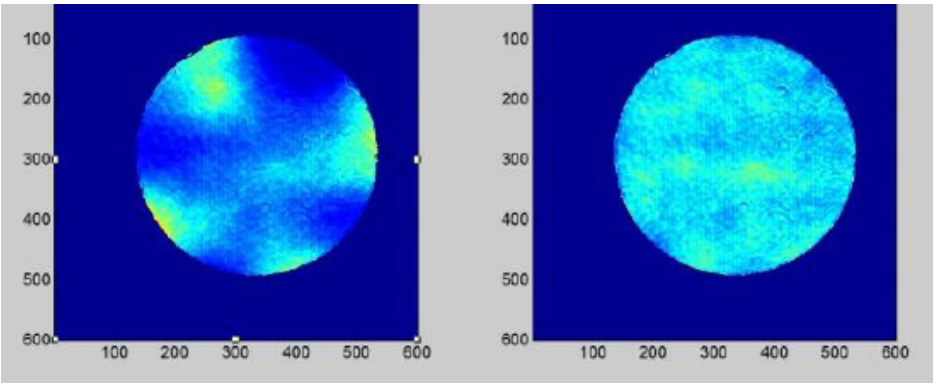

Figure 5. ZELDA images obtained during the LAM demonstration experiment before (left) and after (right) closed-loop correction.

then decomposed on the Zernike polynomial basis, allowing quantitative study of the aberrations present and the influence of the tilt ramp.

Figure 7 shows wavefront maps for two different tilt cases: near zero, corresponding to an estimate of the wavefront seen by the SPHERE infrared coronagraphs (left) and the tilt produced by a 2-pixel (25mas) shift of the source (right). As expected, the latter shows a considerable intensity gradient representing the tilt, but also, towards the left in the image, an inversion of the gradient due to the limited dynamic range of ZELDA as explained in Section 2. This feature imitates a cylindrical wavefront deformation, corresponding to a combination of equal parts of defocus and astigmatism. Figure 8 shows a histogram representation of the variation of the first Zernike modes during this ramp. The variability of focus and astigmatism is clearly seen, and we also see smaller movements in other aberrations, in particular coma and trefoil, imitating the tilt ramp with a five times smaller amplitude.

A closer look at these data is provided by Figure 9 showing estimated tip, tilt, focus and astigmatism coefficients evolving with imposed tilt aberration. It confirms the linear behaviour of the tilt ramp for small aberrations with a gradient slightly below unity, as predicted in our previous paper.[28] The evolution of focus and astigmatism is parabolic, with stationary values around zero tilt.

In Figure 10, the first 36 Zernike coefficients representing the wavefront for close to zero tilt is shown. Ignoring tip, tilt and focus, which are minimized by the coronagraph alignment template before each observation, the wavefront aberration at the infrared coronagraph of SPHERE is dominated by the two astigmatism terms (12 and 22 nm rms respectively) and reaches a total estimated wavefront error of 33 nm rms.

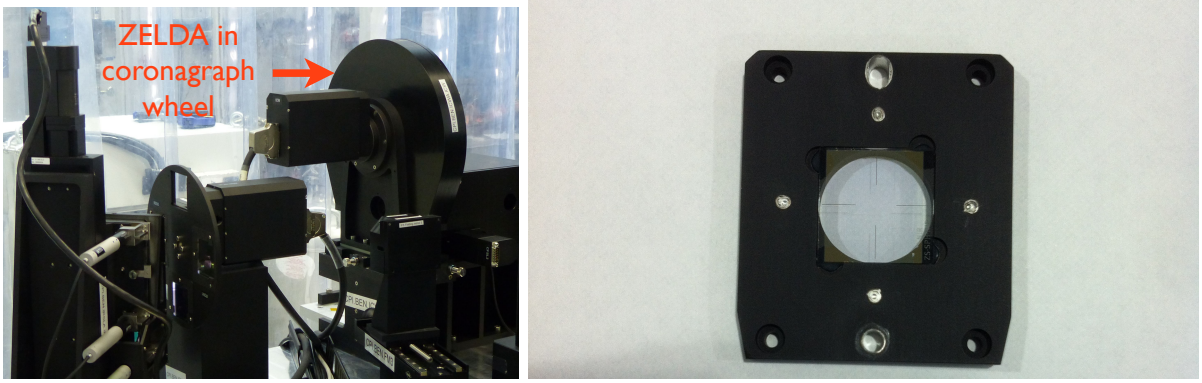

Figure 6. Installation of a ZELDA prototype in the SPHERE coronagraph wheel in April 2014.

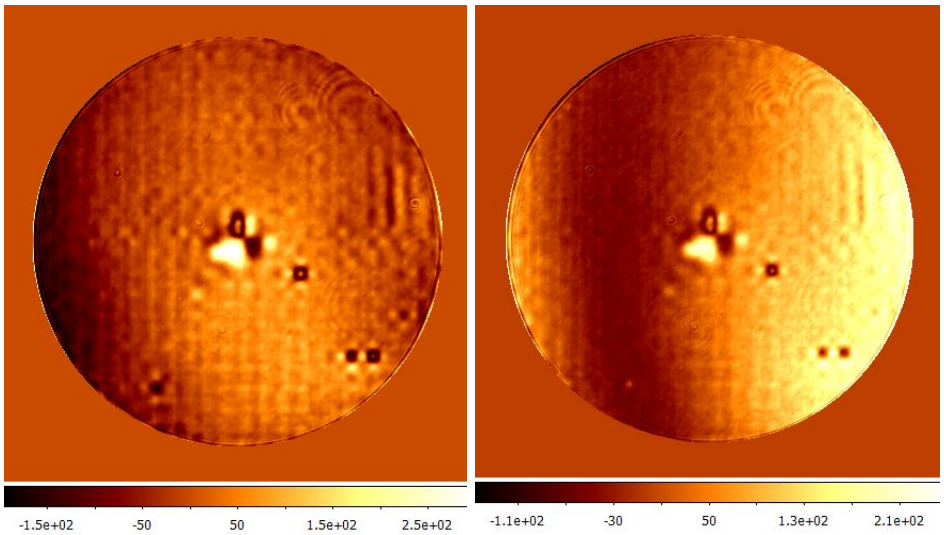

Figure 7. Wavefront maps obtained on SPHERE with ZELDA in the H-band, for near-zero tilt (left) and 2-pixel (25mas) offset (right). The scale is in nm. Data were obtained in May 2014.

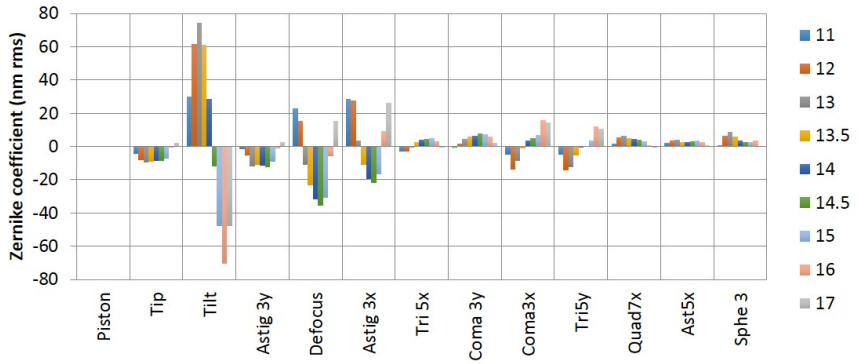

Figure 8. Representation of low-order Zernike aberrations as a function of tilt. The colour code indicates tilt values expressed in terms of spot position in pixels on the SPHERE differential tip-tilt sensor within a 30x30 pixel window. The tilt ramp is clearly observed, saturating as expected when the dynamic range is exceeded. Much smaller movements are seen in other aberration terms, in particular focus and astigmatism showing a parabolic movement, and coma and trefoil imitating the tilt ramp with a five times smaller amplitude.

5. CONCLUSION AND PROSPECTS

More thorough tests of ZELDA on SPHERE are programmed for fall 2014 with the aim to demonstrate reduction of static speckles within the adaptive optics control radius. This is challenging, both in terms of algorithmic interfacing with the SPHERE instrument control software, and in terms of measurement precision and impact of DM defects, amplitude errors, etc. Compared with other methods for NCPA compensation and speckle nulling techniques such as electric field conjugation (EFC) and its avatars[20,21] or coronagraphic phase diversity (COFFEE),[34] which are also foreseen to be tested on SPHERE, major advantages of ZELDA are its rapidity of measurement and simplicity of data processing. Indeed, while EFC requires several hours of calibration and COFFEE typically takes ten minutes of computing time per iteration, ZELDA captures an image and calculates corresponding phase maps in a few seconds.

Common for all these NCPA calibration methods is their inherent off-line nature: aberrations are measured using an internal source at a given moment, and their validity over time relies on the stability of the instrument. While the actual lifetime of speckles for SPHERE in the telescope environment remains to be characterized, an estimation made during SPHERE cold tests[35] estimated an evolution at a rate of 70 pm/min, indicating the need for several calibrations per night. An interesting option offered by the ZELDA concept is to implement it in

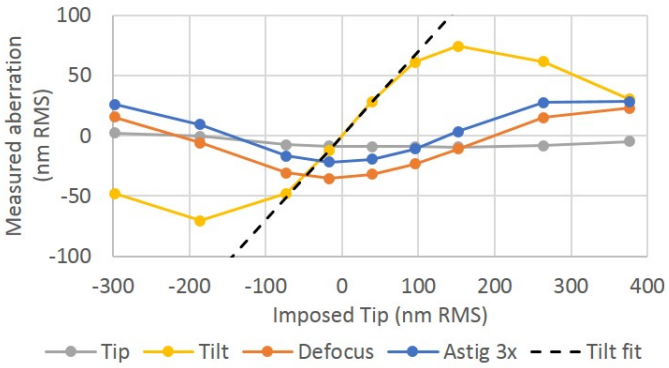

Figure 9. The estimation of tilt with ZELDA is linear over a range of ±100nm rms with a coefficient slightly below unity as expected.[28] The movement seen in tip is probably due to drift during the observation. The parabolic change in focus and astigmatism is caused by the limited range of the ZELDA sensor, as discussed in the text. They are both stationary around zero tilt.

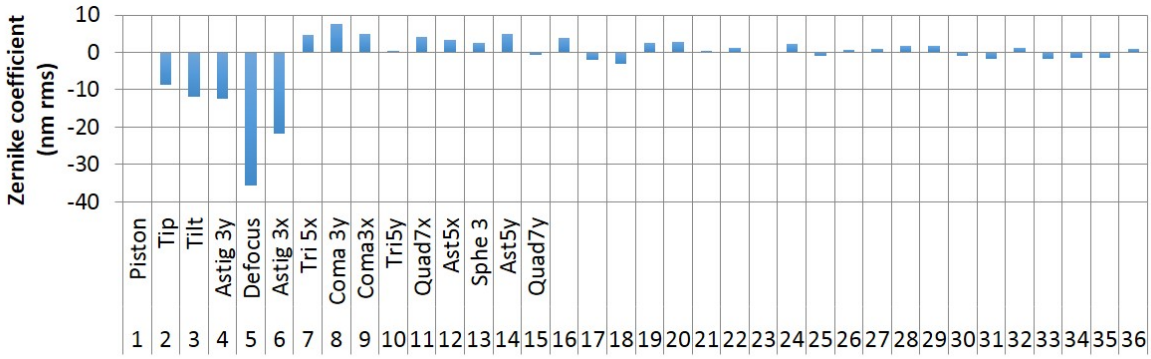

Figure 10. The first 36 Zernike coefficients in the plane of the infrared coronagraph of SPHERE, for near-zero tip-tilt errors, as estimated by ZELDA.

parallel with observations by the aid of a beam splitter taxing a fraction of the science light.[28] In SPHERE such a concept is already implemented in the form of a differential tip-tilt sensor consisting of an auxiliary camera located just upstream of the coronagraphic focus providing on-line calibration of the SPHERE tip-tilt loop at about 0.1 Hz. Implementing ZELDA into this camera, as illustrated in Figure 11 would allow on-line calibration of higher-order aberrations, providing ultimate performance for the instrument. An interesting operational mode for this sensor would be to use it as a stabilizer for dark-hole configurations, possibly obtained using another calibration method such as COFFEE.[34,36]

We are currently also developing a high-contrast imaging testbed at STScI to provide complete solutions in wavefront sensing, wavefront control and starlight suppression with complex aperture telescopes.[37] Recent updates, including design overview and first-light results, are detailed in N'Diaye et al. this conference.[38] This testbed will include low- and mid-order wavefront sensors, possibly based on static (ZELDA) or dynamic Zernike phase mask concepts.[27,28] We have already designed and manufactured a ZELDA prototype for HiCAT testbed to measure wavefront errors in the presence of unfriendly apertures and perform segment fine phasing through a coronagraph. Its implementation will be performed in the forthcoming year.

In the context of direct imaging and spectroscopy of exoplanets, ZELDA could find an application in the future ELTs on the ground, probe-class missions,[39–41] WFIRST-AFTA and its coronagraphic module[42] and the post-JWST flagship mission ATLAST.[43]

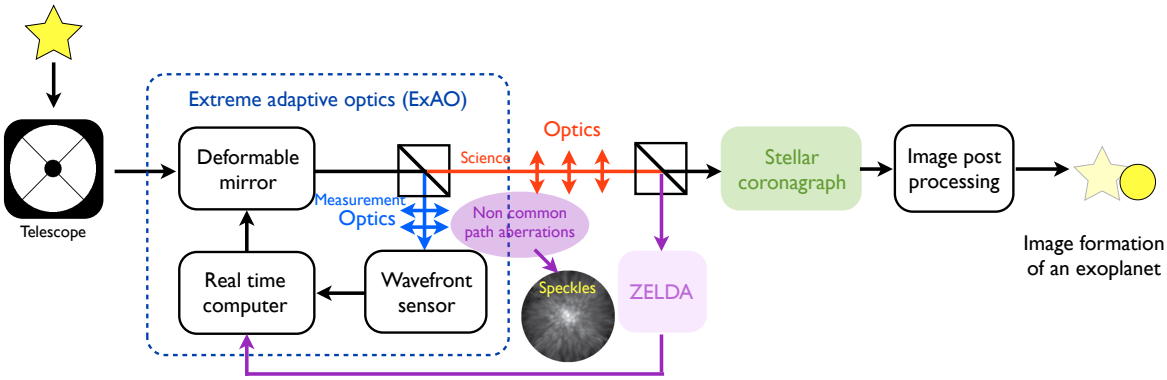

Figure 11. Schematic showing a classical ExAO system (within the blue dotted line) feeding the coronagraph system. Non common path aberrations occur both in the sensing arm (blue arrows) and science path (red arrows). The ZELDA zernike sensor taxes light just upstream of the coronagraph ensuring minimal and stable differential aberrations.

ACKNOWLEDGMENTS

This research was partly supported by funding from CNRS-INSU and the Institute Carnot STAR. The authors acknowledge the Région Provence-Alpes-Côte d'Azur and ONERA for financial support with B. Paul's scholarship. This work was partially based upon work supported by the National Aeronautics and Space Administration under Grant NNX12AG05G issued through the Astrophysics Research and Analysis (APRA) program (Soummer, PI).

REFERENCES

[1] Hinkley, S., Oppenheimer, B. R., Zimmerman, N., Brenner, D., Parry, I. R., Crepp, J. R., Vasisht, G., Ligon, E., King, D., Soummer, R., Sivaramakrishnan, A., Beichman, C., Shao, M., Roberts, L. C., Bouchez, A., Dekany, R., Pueyo, L., Roberts, J. E., Lockhart, T., Zhai, C., Shelton, C., and Burruss, R., "A New High Contrast Imaging Program at Palomar Observatory," *Public. of the Astron. Soc. Pac.* **123**, 74–86 (Jan. 2011).

[2] Macintosh, B., Graham, J. R., Ingraham, P., Konopacky, Q., Marois, C., Perrin, M., Poyneer, L., Bauman, B., Barman, T., Burrows, A., Cardwell, A., Chilcote, J., De Rosa, R. J., Dillon, D., Doyon, R., Dunn, J., Erikson, D., Fitzgerald, M., Gavel, D., Goodsell, S., Hartung, M., Hibon, P., Kalas, P. G., Larkin, J., Maire, J., Marchis, F., Marley, M., McBride, J., Millar-Blanchaer, M., Morzinski, K., Norton, A., Oppenheimer, B. R., Palmer, D., Patience, J., Pueyo, L., Rantakyro, F., Sadakuni, N., Saddlemyer, L., Savransky, D., Serio, A., Soummer, R., Sivaramakrishnan, A., Song, I., Thomas, S., Wallace, J. K., Wiktorowicz, S., and Wolff, S., "The Gemini Planet Imager: First Light," *ArXiv e-prints* (Mar. 2014).

[3] Beuzit, J., Feldt, M., Dohlen, K., Mouillet, D., Puget, P., Wildi, F., Abe, L., Antichi, J., Baruffolo, A., Baudoz, P., Boccaletti, A., Carbillet, M., Charton, J., Claudi, R., Downing, M., Fabron, C., Feautrier, P., Fedrigo, E., Fusco, T., Gach, J., Gratton, R., Henning, T., Hubin, N., Joos, F., Kasper, M., Langlois, M., Lenzen, R., Moutou, C., Pavlov, A., Petit, C., Pragt, J., Rabou, P., Rigal, F., Roelfsema, R., Rousset, G., Saisse, M., Schmid, H., Stadler, E., Thalmann, C., Turatto, M., Udry, S., Vakili, F., and Waters, R., "SPHERE: a planet finder instrument for the VLT," in [*Society of Photo-Optical Instrumentation Engineers (SPIE) Conference Series*], **7014** (Aug. 2008).

[4] Stapelfeldt, K. R., "Extrasolar planets and star formation: science opportunities for future ELTs," in [*The Scientific Requirements for Extremely Large Telescopes*], P. Whitelock, M. Dennefeld, & B. Leibundgut, ed., *IAU Symposium* **232**, 149–158 (2006).

[5] Dohlen, K., Beuzit, J.-L., Feldt, M., Mouillet, D., Puget, P., Antichi, J., Baruffolo, A., Baudoz, P., Berton, A., Boccaletti, A., Carbillet, M., Charton, J., Claudi, R., Downing, M., Fabron, C., Feautrier, P., Fedrigo, E., Fusco, T., Gach, J.-L., Gratton, R., Hubin, N., Kasper, M., Langlois, M., Longmore, A., Moutou, C., Petit, C., Pragt, J., Rabou, P., Rousset, G., Saisse, M., Schmid, H.-M., Stadler, E., Stamm, D., Turatto, M., Waters, R., and Wildi, F., "SPHERE: A planet finder instrument for the VLT," in [*Ground-based and*

Airborne Instrumentation for Astronomy. Edited by McLean, Ian S.; Iye, Masanori. Proceedings of the SPIE, Volume 6269, pp. 62690Q (2006).], **6269** (July 2006).

[6] Fusco, T., Sauvage, J.-F., Petit, C., Costille, C., Mouillet, D., Kasper, M., Dohlen, K., Suarez, M., Baudoz, P., Barrufolo, A., and Beuzit, J.-L., "Final performance and lesson-learned of SAXO, the VLT-SPHERE eXtreme AO: from early design to on-sky results," in [*Society of Photo-Optical Instrumentation Engineers (SPIE) Conference Series*], **9148** (2014).

[7] Marois, C., Doyon, R., Racine, R., and Nadeau, D., "Efficient Speckle Noise Attenuation in Faint Companion Imaging," *Public. of the Astron. Soc. Pac.* **112**, 91–96 (Jan. 2000).

[8] Sparks, W. B. and Ford, H. C., "Imaging Spectroscopy for Extrasolar Planet Detection," *Astrophysical Journal* **578**, 543–564 (Oct. 2002).

[9] Marois, C., Lafrenière, D., Doyon, R., Macintosh, B., and Nadeau, D., "Angular Differential Imaging: A Powerful High-Contrast Imaging Technique," *Astrophysical Journal* **641**, 556–564 (Apr. 2006).

[10] Lafrenière, D., Marois, C., Doyon, R., Nadeau, D., and Artigau, É., "A New Algorithm for Point-Spread Function Subtraction in High-Contrast Imaging: A Demonstration with Angular Differential Imaging," *Astrophysical Journal* **660**, 770–780 (May 2007).

[11] Soummer, R., Pueyo, L., and Larkin, J., "Detection and Characterization of Exoplanets and Disks Using Projections on Karhunen-Loève Eigenimages," *Astrophysical Journal, Letters* **755**, L28 (Aug. 2012).

[12] Pueyo, L., Crepp, J. R., Vasisht, G., Brenner, D., Oppenheimer, B. R., Zimmerman, N., Hinkley, S., Parry, I., Beichman, C., Hillenbrand, L., Roberts, L. C., Dekany, R., Shao, M., Burruss, R., Bouchez, A., Roberts, J., and Soummer, R., "Application of a Damped Locally Optimized Combination of Images Method to the Spectral Characterization of Faint Companions Using an Integral Field Spectrograph," *Astrophysical Journal, Supplement* **199**, 6 (Mar. 2012).

[13] Sauvage, J.-F., Fusco, T., Rousset, G., and Petit, C., "Calibration and precompensation of noncommon path aberrations for extreme adaptive optics," *Journal of the Optical Society of America A* **24**, 2334–2346 (Aug. 2007).

[14] Mugnier, L. M., Sauvage, J.-F., Fusco, T., Cornia, A., and Dandy, S., "On-Line Long-Exposure Phase Diversity: a Powerful Tool for Sensing Quasi-Static Aberrations of Extreme Adaptive Optics Imaging Systems," *Optics Express* **161**, 18406–18416 (Oct. 2008).

[15] Paul, B., Sauvage, J.-F., and Mugnier, L. M., "Coronagraphic phase diversity: performance study and laboratory demonstration," *Astron. & Astrophys.* **552**, A48 (Apr. 2013).

[16] Wallace, J. K., Burruss, R. S., Bartos, R. D., Trinh, T. Q., Pueyo, L. A., Fregoso, S. F., Angione, J. R., and Shelton, J. C., "The Gemini Planet Imager calibration wavefront sensor instrument," in [*Society of Photo-Optical Instrumentation Engineers (SPIE) Conference Series*], **7736** (July 2010).

[17] Galicher, R., Baudoz, P., and Rousset, G., "Wavefront error correction and Earth-like planet detection by a self-coherent camera in space," *Astron. & Astrophys.* **488**, L9–L12 (Sept. 2008).

[18] Galicher, R., Baudoz, P., Rousset, G., Totems, J., and Mas, M., "Self-coherent camera as a focal plane wavefront sensor: simulations," *Astron. & Astrophys.* **509**, A31 (Jan. 2010).

[19] Bordé, P. J. and Traub, W. A., "High-Contrast Imaging from Space: Speckle Nulling in a Low-Aberration Regime," *Astrophysical Journal* **638**, 488–498 (Feb. 2006).

[20] Give'on, A., Kern, B., Shaklan, S., Moody, D. C., and Pueyo, L., "Electric Field Conjugation - A Broadband Wavefront Correction Algorithm For High-contrast Imaging Systems," in [*American Astronomical Society Meeting Abstracts*], *Bulletin of the American Astronomical Society* **39**, 135.20 (Dec. 2007).

[21] Pueyo, L., Kay, J., Kasdin, N. J., Groff, T., McElwain, M., Give'on, A., and Belikov, R., "Optimal dark hole generation via two deformable mirrors with stroke minimization," *Appl. Opt.* **48**, 6296–6312 (Nov 2009).

[22] Guyon, O., Matsuo, T., and Angel, R., "Coronagraphic Low-Order Wave-Front Sensor: Principle and Application to a Phase-Induced Amplitude Coronagraph," *Astrophysical Journal* **693**, 75–84 (Mar. 2009).

[23] Vogt, F. P. A., Martinache, F., Guyon, O., Yoshikawa, T., Yokochi, K., Garrel, V., and Matsuo, T., "Coronagraphic Low-Order Wavefront Sensor: Postprocessing Sensitivity Enhancer for High-Performance Coronagraphs," *Public. of the Astron. Soc. Pac.* **123**, 1434–1441 (Dec. 2011).

[24] Zernike, F., "Diffraction theory of the knife-edge test and its improved form, the phase-contrast method," *Mon. Not. of the Royal Astron. Soc.* **94**, 377–384 (Mar. 1934).

[25] Bloemhof, E. E. and Wallace, J. K., "Phase contrast techniques for wavefront sensing and calibration in adaptive optics," in [*Society of Photo-Optical Instrumentation Engineers (SPIE) Conference Series*], Tyson, R. K. and Lloyd-Hart, M., eds., **5169**, 309–320 (Dec. 2003).

[26] Dohlen, K., "Phase masks in astronomy: From the Mach-Zehnder interferometer to coronagraphs," in [*EAS Publications Series*], Aime, C. and Soummer, R., eds., **12**, 33–44 (2004).

[27] Wallace, J. K., Rao, S., Jensen-Clem, R. M., and Serabyn, G., "Phase-shifting Zernike interferometer wavefront sensor," in [*Society of Photo-Optical Instrumentation Engineers (SPIE) Conference Series*], **8126** (Sept. 2011).

[28] N'Diaye, M., Dohlen, K., Fusco, T., and Paul, B., "Calibration of quasi-static aberrations in exoplanet direct-imaging instruments with a Zernike phase-mask sensor," *Astron. & Astrophys.* **555**, A94 (July 2013).

[29] N'Diaye, M., Dohlen, K., Fusco, T., El Hadi, K., Soummer, R., Cuevas, S., Zerrad, M., and Ferrari, M., "Lab results of the circular phase mask concepts for high-contrast imaging of exoplanets," in [*Society of Photo-Optical Instrumentation Engineers (SPIE) Conference Series*], *Society of Photo-Optical Instrumentation Engineers (SPIE) Conference Series* **8450** (Sept. 2012).

[30] Dohlen, K., Madec, F., N'Diaye, M., Paul, B., Fusco, T., Jolivet, A., Luo, D., Yatcheva, L., Sauvage, J.-F., Mugnier, L., and Ferrari, M., "Lab demonstration of the Zernike phase mask near-coronagraph quasi static aberrations sensor, ZELDA," in [*Proceedings of the Third AO4ELT Conference*], Esposito, S. and Fini, L., eds. (Dec. 2013).

[31] Roddier, F. and Roddier, C., "Stellar Coronograph with Phase Mask," *Public. of the Astron. Soc. Pac.* **109**, 815–820 (July 1997).

[32] Guyon, O. and Roddier, F. J., "Direct exoplanet imaging possibilities of the nulling stellar coronagraph," in [*Proc. SPIE Vol. 4006, p. 377-387, Interferometry in Optical Astronomy, Pierre J. Lena; Andreas Quirrenbach; Eds.*], Lena, P. J. and Quirrenbach, A., eds., *Presented at the Society of Photo-Optical Instrumentation Engineers (SPIE) Conference* **4006**, 377–387 (July 2000).

[33] Soummer, R., Aime, C., and Falloon, P. E., "Stellar coronagraphy with prolate apodized circular apertures," *Astron. & Astrophys.* **397**, 1161–1172 (Jan. 2003).

[34] Paul, B., Sauvage, J.-F., Mugnier, L. M., Dohlen, K., Petit, C., Fusco, T., Mouillet, D., Beuzit, J.-L., and Ferrari, M., "Compensation of high-order quasi-static aberrations on SPHERE with the coronagraphic phase diversity (COFFEE)," *Astron. & Astrophys.* , to appear (2014).

[35] Martinez, P., Kasper, M., Costille, A., Sauvage, J. F., Dohlen, K., Puget, P., and Beuzit, J. L., "Speckle temporal stability in XAO coronagraphic images. II. Refine model for quasi-static speckle temporal evolution for VLT/SPHERE," *Astron. & Astrophys.* **554**, A41 (June 2013).

[36] Sauvage, J.-F., Mugnier, L., Paul, B., and Villecroze, R., "Coronagraphic phase diversity: a simple focal plane sensor for high-contrast imaging," *Optics Letters* **37**, 4808 (Dec. 2012).

[37] N'Diaye, M., Choquet, E., Pueyo, L., Elliot, E., Perrin, M. D., Wallace, J. K., Groff, T., Carlotti, A., Mawet, D., Sheckells, M., Shaklan, S., Macintosh, B., Kasdin, N. J., and Soummer, R., "High-contrast imager for complex aperture telescopes (HiCAT): 1. testbed design," in [*Society of Photo-Optical Instrumentation Engineers (SPIE) Conference Series*], **8864** (Sept. 2013).

[38] N'Diaye, M., Choquet, E., Egron, S., Pueyo, L., Leboulleux, L., Levecq, O., Perrin, M. D., Elliot, E., Wallace, J. K., Long, C., Anderson, R., DiFelice, A., and Soummer, R., "High-contrast imager for complex aperture telescopes (HiCAT): 2. design overview and first light results," in [*Society of Photo-Optical Instrumentation Engineers (SPIE) Conference Series*], **9143** (2014).

[39] Trauger, J., Stapelfeldt, K., Traub, W., Krist, J., Moody, D., Mawet, D., Serabyn, E., Henry, C., Brugarolas, P., Alexander, J., Gappinger, R., Dawson, O., Mireles, V., Park, P., Pueyo, L., Shaklan, S., Guyon, O., Kasdin, J., Vanderbei, R., Spergel, D., Belikov, R., Marcy, G., Brown, R. A., Schneider, J., Woodgate, B., Egerman, R., Matthews, G., Elias, J., Conturie, Y., Vallone, P., Voyer, P., Polidan, R., Lillie, C., Spittler, C., Lee, D., Hejal, R., Bronowicki, A., Saldivar, N., Ealey, M., and Price, T., "ACCESS: a concept study for the direct imaging and spectroscopy of exoplanetary systems," in [*Society of Photo-Optical Instrumentation Engineers (SPIE) Conference Series*], **7731** (July 2010).

[40] Guyon, O., Shaklan, S., Levine, M., Cahoy, K., Tenerelli, D., Belikov, R., and Kern, B., "The pupil mapping exoplanet coronagraphic observer (PECO)," in [*Society of Photo-Optical Instrumentation Engineers (SPIE) Conference Series*], **7731** (July 2010).

[41] Boccaletti, A., Schneider, J., Traub, W., Lagage, P.-O., Stam, D., Gratton, R., Trauger, J., Cahoy, K., Snik, F., Baudoz, P., Galicher, R., Reess, J.-M., Mawet, D., Augereau, J.-C., Patience, J., Kuchner, M., Wyatt, M., Pantin, E., Maire, A.-L., VÃ©rinaud, C., Ronayette, S., Dubreuil, D., Min, M., Rodenhuis, M., Mesa, D., Belikov, R., Guyon, O., Tamura, M., Murakami, N., and Beerer, I., "Spices: spectro-polarimetric imaging and characterization of exoplanetary systems," *Experimental Astronomy* , 1–30 (2012). 10.1007/s10686-012-9290-5.

[42] Spergel, D., Gehrels, N., Breckinridge, J., Donahue, M., Dressler, A., Gaudi, B. S., Greene, T., Guyon, O., Hirata, C., Kalirai, J., Kasdin, N. J., Moos, W., Perlmutter, S., Postman, M., Rauscher, B., Rhodes, J., Wang, Y., Weinberg, D., Centrella, J., Traub, W., Baltay, C., Colbert, J., Bennett, D., Kiessling, A., Macintosh, B., Merten, J., Mortonson, M., Penny, M., Rozo, E., Savransky, D., Stapelfeldt, K., Zu, Y., Baker, C., Cheng, E., Content, D., Dooley, J., Foote, M., Goullioud, R., Grady, K., Jackson, C., Kruk, J., Levine, M., Melton, M., Peddie, C., Ruffa, J., and Shaklan, S., "Wide-Field InfraRed Survey Telescope-Astrophysics Focused Telescope Assets WFIRST-AFTA Final Report," *ArXiv e-prints* (May 2013).

[43] Postman, M., Brown, T., Sembach, K., Giavalisco, M., Traub, W., Stapelfeldt, K., Calzetti, D., Oegerle, W., Michael Rich, R., Phillip Stahl, H., Tumlinson, J., Mountain, M., Soummer, R., and Hyde, T., "Advanced Technology Large-Aperture Space Telescope: science drivers and technology developments," *Optical Engineering* **51**, 011007 (Jan. 2012).